FLOW CHARACTERISTICS BEYOND TIME AND PHASE
A MODAL ANALYSIS OF THE PATTERNS IN A REGENERATIVE PUMP

Philipp MATTERN[1], Jochen KRIEGSEIS[2], Martin GABI[1]

[1] *Institute of Fluid Machinery (FSM)*

[2] *Institute of Fluid Mechanics (ISTM)*

KIT, Kaiserstraße 12, 76131 Karlsruhe, Germany

SUMMARY

The purpose of this paper is to introduce the proper orthogonal decomposition (POD) as an efficient method to understand the complex flow behavior of fluid machinery in case of appearing periodicity. Despite progressively mature application for reduced-order-model approaches (ROM), only little attention is paid to POD as a tool for pattern identification and subsequent intensity quantification. The *hidden beauty* [1] of this method for fluid/turbo machinery is emphasized in the present manuscript, with the main focus on a complementary discussion of conventional post processing (time and phase average, qualitative topology analysis) and the POD approach. The discussion is supported by high-speed 2D-3C PIV measurement data within the side channel of a regenerative pump, which reveals the interaction between the side channel and the impeller.

INTRODUCTION

Nowadays, advanced optical non-intrusive measurement methods [2, 3] allow a deeper insight into rather complex flow fields, which in the present case is the fluid-blade interaction inside fluid machinery. Particularly, the side channel above a regenerative pump (Figure1) is considered.

A common method to do this, is to use Particle Image Velocimetry for the acquisition of (most commonly) two dimensional (2D) flow field information with either two (2C) or all three (3C) velocity components (Given that sufficient hardware is at hand, this decision is closely influenced by the flow scenario under

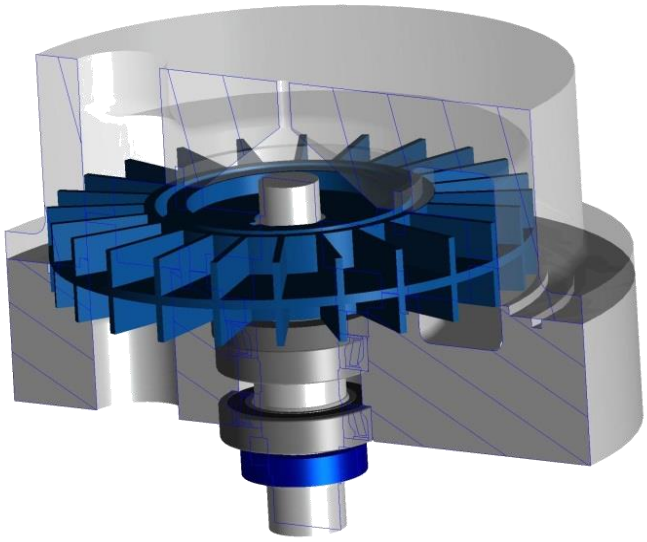

Figure 1: CAD Model of the regenerative pump

consideration, setup situation, feasibility, optical accessibility, etc.).

Once obtained and post-processed, a common standard approach for the flow field analysis is the determination of a temporal and/or spatial average of the data [4,5,6,7]. Moreover, combined approaches like phase averaging have been proven to be very beneficial for periodic flows. However, the major disadvantage of a phase averaging approach is the dependency on a specific frequency, either manually chosen, or deduced from signal processing efforts. Regarding fluid machinery, this frequency is commonly related to the rotational speed of the machine or any other frequency being a multiple of this base frequency (e.g. blade passing frequency). As a consequence, only flow phenomena related to this frequency can be revealed by this method, leaving any non-rotational speed related phenomena hidden in the phase averaged results (e.g. the complex oscillating phenomena of a rotating stall [8,9]). Nevertheless, since most fluid machinery phenomena do in fact relate to the rotational speed (or harmonics), this approach already allows a profound understanding of the flow within the machine and has been proven reliable for a long time.

As for time resolved data, it is common to analyze the velocity components by matters of trends, periodicity and frequencies [10,11]. Although normally more common when using single point optical measurement, such as Laser-Doppler anemometry, it also can be done for field measurements methods like PIV. Yet, a special challenge in this case is to find an adequate solution in presenting the vast amount of information when combining an already information-heavy field technique with additional time information. One approach could be to extract information from a single point within the field, study the temporal evolvement and confirm the drawn conclusions by manually selected additional points within the field. Besides that, temporal behavior is often described by showing only a few snapshots of a given sequence to make the temporal behavior more understandable to the reader. Regardless of the used technique, post-processing is work-intensive, time consuming and requires high presentation skills to transport the desired significance of the message clearly.

Another approach to post-process and analyze flow field data is the proper orthogonal decomposition (POD) [1,12,13]. By decomposing the flow field into its spatial POD modes, dominant flow structures can be described and quantified. In other words: the flow field is decomposed into energy- weighted flow patterns. By definition, these flow patterns are linearly independent, therefore neither linked to each other, nor depending on a common frequency, enabling a significantly deeper understanding of the flow, as no common base is needed. Furthermore, analysis of only a few dominant basic flow patterns saliently uncovers the dynamics of the flow. Finally, the flow field can be reconstructed only using the strongest of these patterns, which on one hand represent a filtering approach and on the other hand enables to predict similar flow scenarios by means of so-called reduced order models (both beyond the scope of the present manuscript).

Motivation for the present paper originated from processing issue with the above-mentioned vast amounts of spatiotemporal velocity information, obtained with a high-speed stereo PIV (HS-SPIV) system. Measurements were done to analyze the complex flow through the side channel of regenerative pump at a position, where the flow field was assumed to be fully developed. Of peculiar interest was the identification of the coherent flow patterns involved. Due to the complexity of the test rig, the measurement setup and the nature of the flow, results were slightly noisy. Common approaches in analyzing the data resulted in averaged flow fields, only giving limited insight into the flow field. Here, the additional application of the POD revealed a significantly deeper understanding of the complex flow behavior of the machine. Based on this complementary analysis, a more profound understanding of the working principle of the pump was possible as will be discussed in the present work.

EXPERIMENTAL SETUP

Figure 1 shows the generic model. The impeller with its 24 blades and a diameter of 200 mm is covered by an acrylic casing with the side channel integrated. Although a double flow machine was realized due to symmetrical reasons, only the upper flow was examined. The machine is running at a speed of 500 rpm. The common layout of the test rig allows full control over the flow regime and therefore the operation point of the machine. Flow direction through the machine, field of view and the chosen coordinate system are indicated in Figure 2. The fluid enters the machine at the upper right corner and is circularly transported along Θ through the side channel to the outlet (This defines the main flow). z defines the axial coordinate, while Θ and r are the radial and circumferential coordinates, respectively. Note that in- and outlet are separated by a stripper (hatched area), with its center being used as the origin for the Θ coordinate. The rotation axis defines the origin for r, while the axial tip of the blades defines the origin for z. The light sheet of the laser enters the acrylic casing from the left and illuminates the area marked in red. Even though not shown in the present work, it is worth to note, that all PIV experiments were simultaneously monitored with more common methods as well, all synced to the same time signal. Pressure probes were installed to take the static wall pressure near the in- and outlet of the machine. Additionally, torque, as well as rpm and angular position of the impeller were measured.

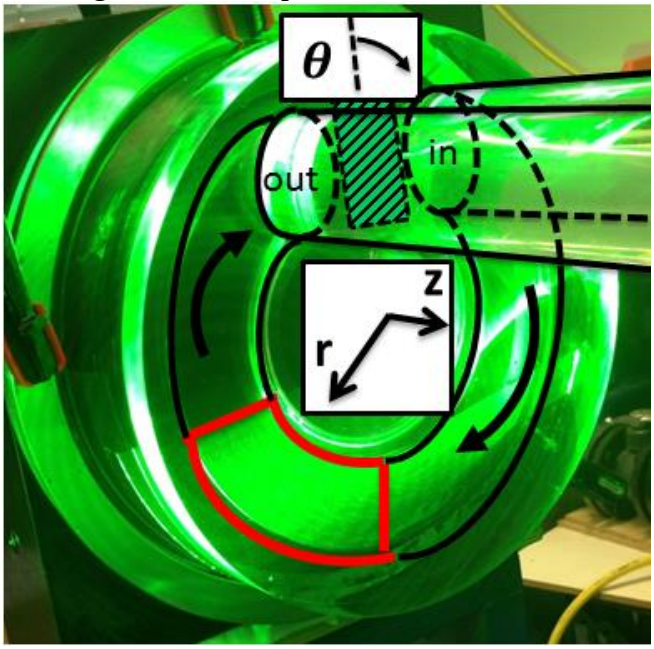

Figure 2: Acrylic Side Channel with marked PIV Measurement Position (red area)

Although the campaign covered various impeller designs, different operating points and different measurement planes, this paper is only using the near-impeller plane (2mm) for the 24 blade impeller near its best operating point to elaborate the different approaches.

The transport mechanism of the machine is described by an axial interaction between the flow in the side channel and the blades of the impeller (secondary flow). This secondary flow is shown in red in Figure 3. The Stereo PIV System is set up in a standard Forward/Backward scattered Setup, with an angle of 65° between both cameras and a distance of 340 mm between the cameras and the light sheet. The flow is captured at 2000 fps with a resolution of 1 Megapixel. More details of the experimental setup can be found in [14,15].

POST-PROCESSING

For PIV Analysis PIVTEC's PIVview (V3.5.9.1) is used. Common methods of dewarping and disparity correction are applied. The cross correlation has an interrogation area of 16x16 pixels and an overlap of 50%. A strict dynamic mean filter of 2*mean velocity ± 1*standard deviation leads to a small amount of around 0.5% invalid vectors which could

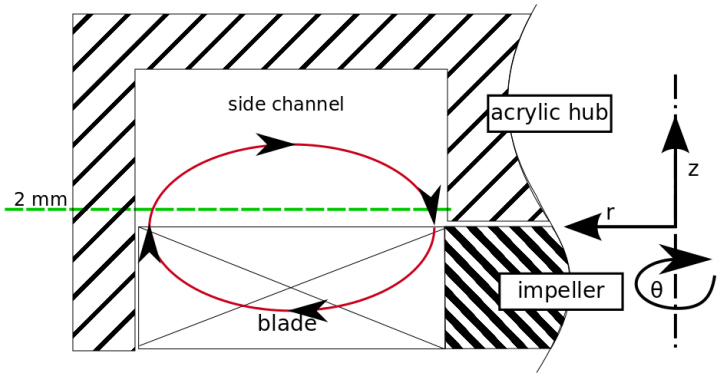

Figure 3: Measurement planes (dotted green) with superimposed secondary flow (red)

nearly all be replaced by their second highest correlation peaks. Separation time (pulse distance) between the two pulses is 100 µs. During 1.4 seconds of measurement, *N = 2771* velocity maps for an area of 110x50 mm each containing around 3000 three component vectors are captured. Customized post-processing algorithms have been applied for any further analysis of the velocity data.

TIME- AND/OR PHASE-AVERAGED RESULTS

In a first approach the resulting vector maps are time averaged as shown in Figure 4. The average in-plane velocity is approximately $\bar{c} = 3\,m/s$, which is significantly higher than the axial component (-0.8 to 0.4 m/s) shown as the contour plot. To improve readability, a magenta line marks the zero crossing of the axial (secondary) flow in this figure, as well as where needed below.

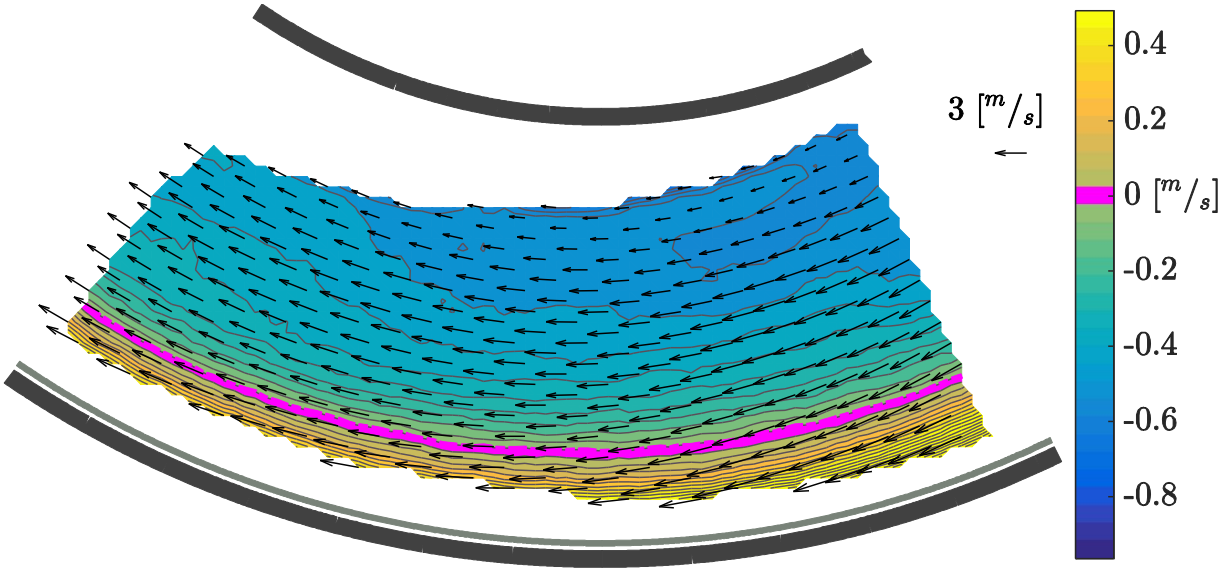

Figure 4: Absolute velocity components for a specific angle: in-plane as vectors, (out-of-plane) as contours

The high circumferential velocity describes the main volume flow through the side channel at the present operating point. As expected, the axial flow direction changes over the radius. It shows backflow into the impeller for small radii up to ¾ of the side channel (axial zero crossing in magenta). At that point, axial flow direction switches, henceforth rapidly increasing up to the outer rim.

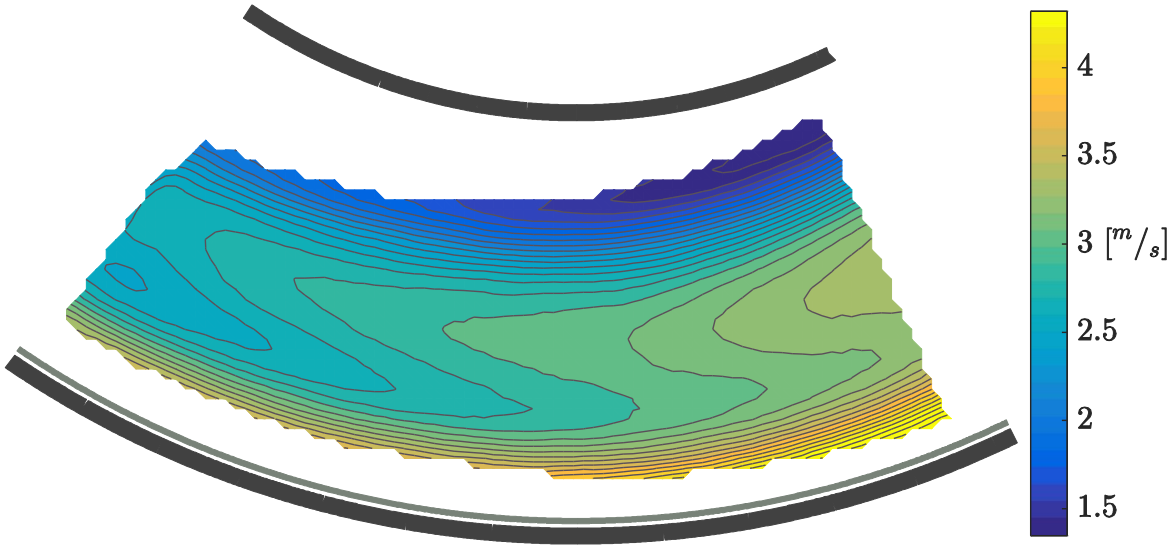

Figure 5: Absolute velocity magnitude

Figure 5 shows the velocity magnitude. Coming from very low velocities near the hub, it stays quite constant along *r*, suddenly increasing when the axial zero crossing is passed (see magenta line Figure 4) towards the outer rim. Along the quite constant middle section of the side channel, velocity is slowly decreasing in the direction of rotation.

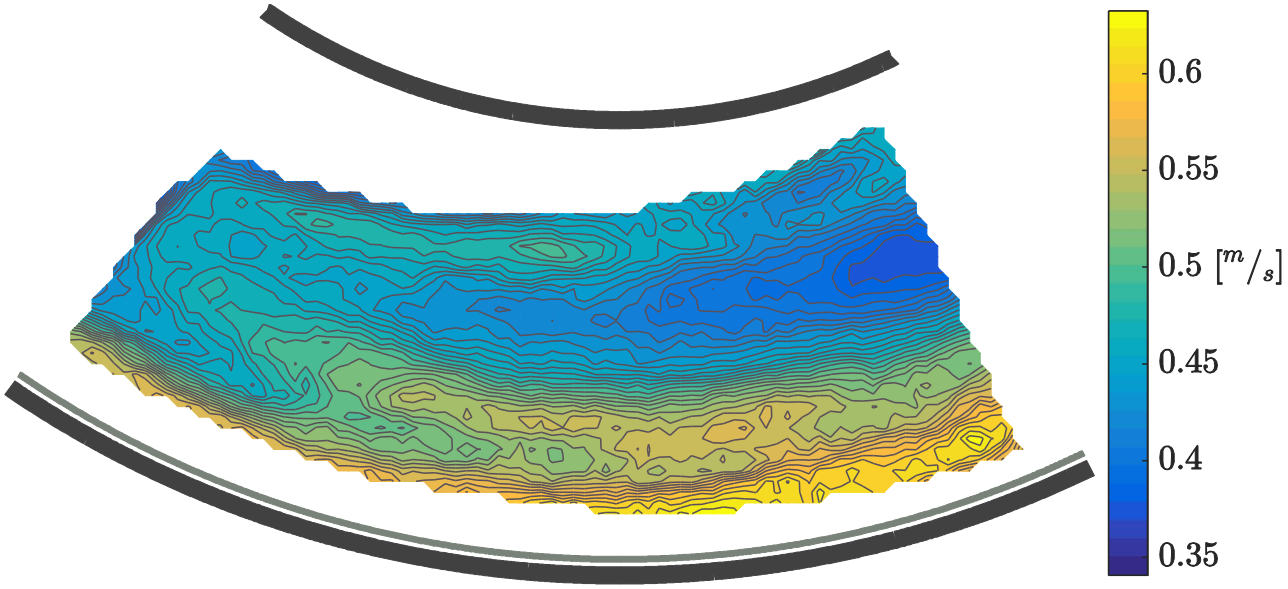

Figure 6: Standard deviation (STD) of absolute magnitude

Figure 6 shows the standard deviation (STD) of the magnitude for each point. It indicates that the fluctuations at the outer rim of the side channel are approximately twice as high as in the inner part. Figure 7 shows the ratio of STD and average. The structure resembles the structure of the STD, showing its strong influence on the pattern. However, it is now revealed that the ratio is only strong near the hub, while being quite homogenously distributed at the rest of the field. Any blade related velocity patterns are annihilated due to the temporal averaging.

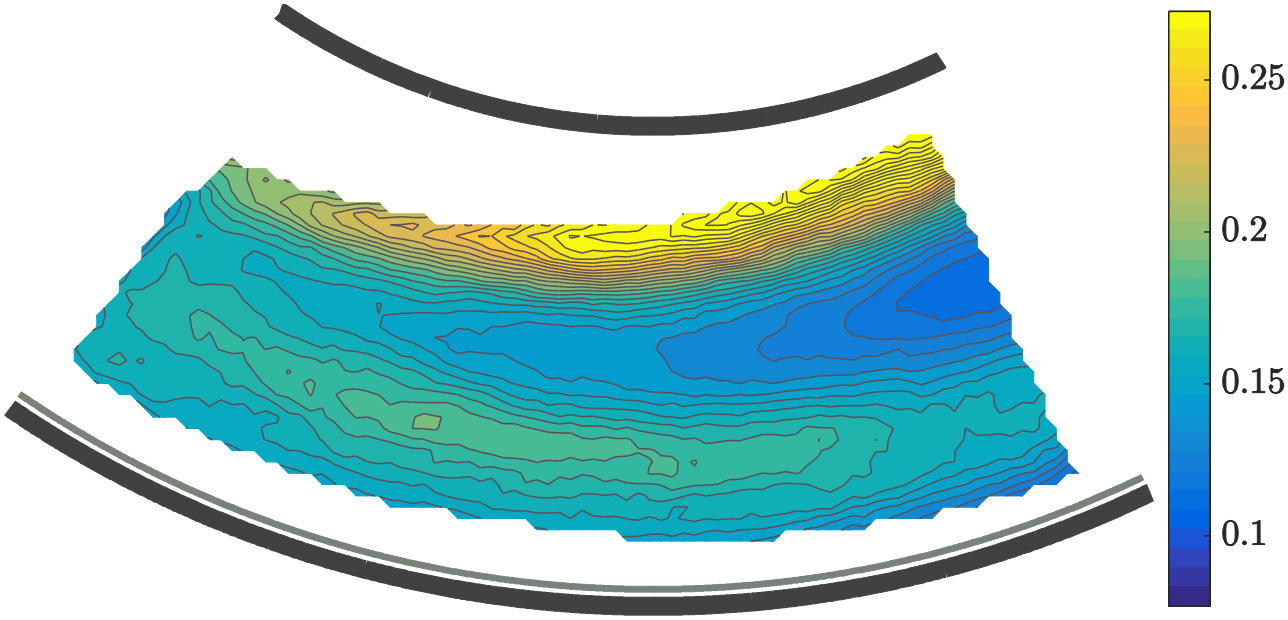

Figure 7: Ratio of STD and average

By using the angular position of the impeller as additional information, it is possible to do a phase averaging for a fixed position of the impeller. Figure 8 shows such a phase averaged flow field

with all three components of the velocity, as well as the underlying blades (Recall, that the shown flow field is 2 mm above the impeller).

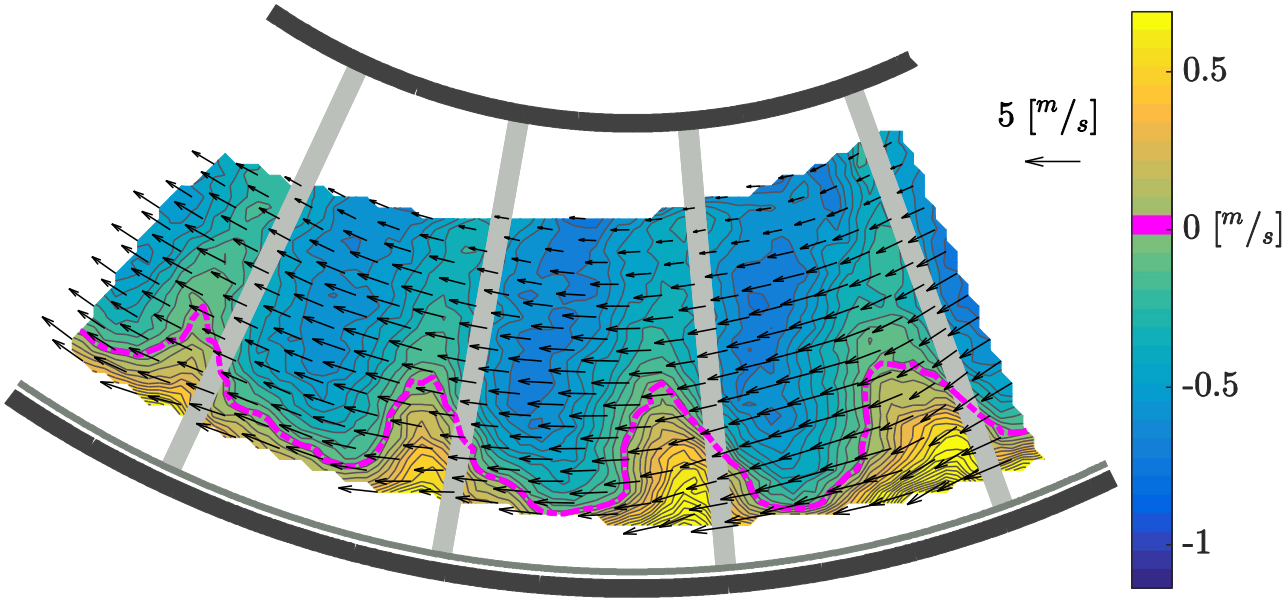

Figure 8: Phaseaveraged absolute velocity components for a specific angle: inplane as vectors, axial as contours

It is noticeable that the in-plane components (~5m/s; see Reference vector) are one order of magnitude stronger than the out of plane components (-0.5 to 0.5 m/s). It now becomes visible that the flow within the side channel is strongly influenced by the blades, revealing a pattern-like structure moving along with θ. Furthermore, a salient wavelike structure of the main flow is now uncovered at the outer wall. Although around 280 velocity maps were averaged for each phase-point, there remain considerable amounts of noise.

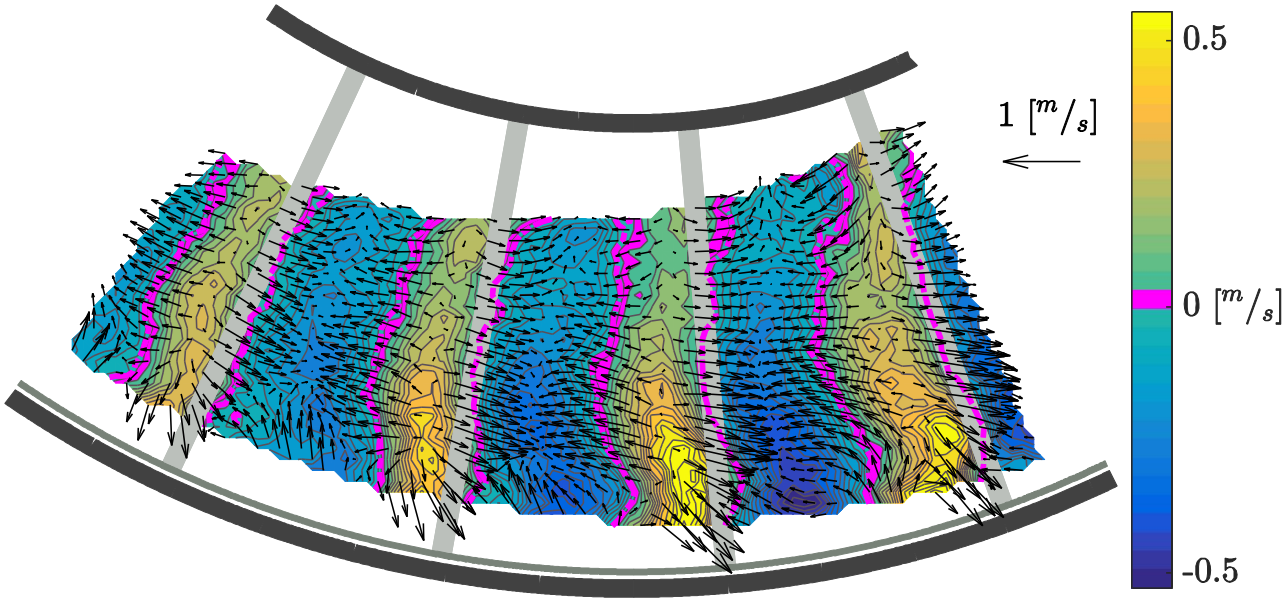

Figure 9: Phaseaveraged absolute velocity (Figure 8) subtracted by mean absolute velocity (Figure 4)

Figure 9 introduces the approach to subtract the time averaged mean flow field (see Figure 4) from the phase averaged flow field (see Figure 8). Now that the predominant average flow is suppressed, the working principle of the machine reveals. While the impeller is rotating, the fluid has to evade the blade by streaming into the side channel in axial direction (warm colors), as well in-plane in radial direction. In addition, there's also an in-plane flow visible from the pressure side (warm

colors) to the suction side (cool colors) above each blade channel. Furthermore, a flow over the blades from pressure- to suction side in circumferential direction becomes obvious from this diagram. Due to the nature of the flow, complex vortices at the outer diameter, as well as near the hub can be assumed.

To investigate the blade related structure furthermore and with the local circumferential velocity ($\omega * r$) at each point given as additional information, it is now possible to switch from the laboratory frame of reference (absolute velocity c) to the blade-fixed frame of reference (relative velocity w). The relative circumferential velocity ($w_u = c_u - u$) is shown in Figure 10.

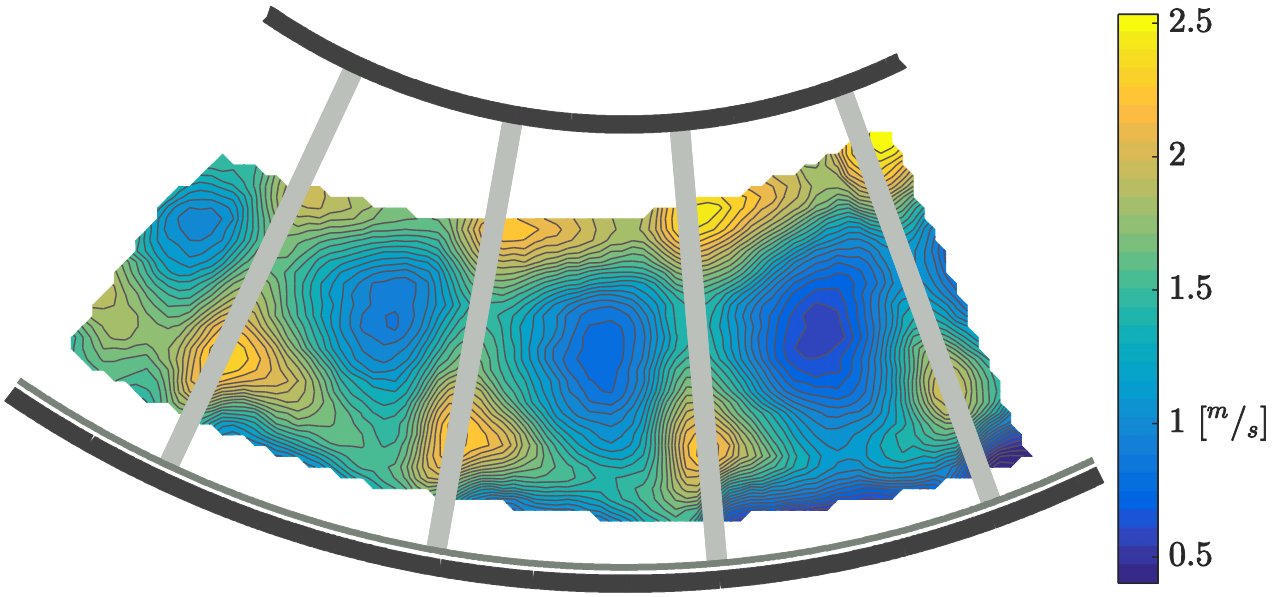

Figure 10: Phaseaveraged relative circumferential velocity (w_u)

It reveals a rather counter-intuitive complex flow field. Again, the number of similar pattern is directly related to the number of blades. Nonetheless, an obvious explanation of the resulting flow field related to the blade geometry is not possible beyond such visual trends.

As an intermediate conclusion, common approaches are indeed capable to uncover some salient patterns and corresponding dynamics from flow fields. Time averaging reveals the underlying secondary flow: The high positive axial velocities at the outer rim on the pressure side of the blade can be explained, as the fluid is blocked by the casing. Consequently, it cannot be transported furthermore along the radius and therefore has to evade upwards into the side channel. The necessary negative backflow into the blade channel is now more obvious. Phase averaging refines the flow field even further: Blade related structures can be identified. It becomes obvious that the flow itself is quite complex and that in addition to the secondary flow there are further periodic flow mechanism within the machine. As phase averaging is only suitable for periodic phenomena, it is necessary to assume a characteristic frequency. In case of fluid machinery the blade frequency is sufficient in most of the cases. A huge drawback of such processing approaches is the limitation to the preset frequency, as only periodical phenomena with this distinct frequency can be observed. Another more flexible approach to understand the complex flow situation furthermore is the POD, as illustrated below.

BASICS: PROPER ORTHOGONAL DECOMPOSITION (POD)

In order to uncover coherent structures embedded in the flow, the data was decomposed by means of proper orthogonal decomposition (POD). A brief introduction into POD is provided below, adapted from Kriegseis *et al.* [16] and Fernando *et al.* [17].

Unsteady velocity information $\widetilde{U}(\vec{x},t)$ can be decomposed into its average and transient components, as shown in the Reynolds decomposition $\widetilde{U}(\vec{x},t^i) = \bar{u}(\vec{x}) + u(\vec{x},t^i)$ for time step t^i. In general, a POD separates spatially correlated but temporally inhomogeneous flow structures from uncorrelated random fluctuations (noise), both of which are contained in the deviations $u(\vec{x},t^i)$. These deviations u^i from the mean form a covariance matrix $R = UU^T$, where $U = [u^1, u^2 \dots u^N]$. The solution of the eigenvalue problem $R\Phi = \lambda\Phi$ leads to the POD Modes ϕ_j (eigenvectors) with corresponding eigenvalues λ_j. These Modes in fact reveal coherent flow patterns superimposed to the mean flow field. The resulting contribution of each mode j to the overall signal power is given by $P_j = \lambda_j / \|\lambda\|$. Since the eigenvalues are ordered decreasingly, the first few Modes ϕ_j of the matrix $\Phi = [\phi_1, \phi_2 \dots \phi_N]^T$ typically contain the main part of the energy in the recorded flow scenario. The impact of each Mode ϕ_j to the individual snap shots u^i can be determined in terms of the weighting coefficients $a_j^i = \phi_j u^i$. Note that the average $\overline{a_j}$ of a_j^i over N snapshots is zero by definition, i.e. $\overline{a_j} = \frac{1}{N}\sum_{i=1}^{N} a_j^i := 0$. In contrast, the standard deviations $\sigma_j = \sqrt{\frac{1}{N-1}\sum_{i=1}^{N}\left(a_j^i\right)^2}$ are non-zero and indicate the fluctuation intensity of Mode ϕ_j.

Is has to be mentioned, that POD is described in the common form. Therefore the general notation of $\widetilde{U}(\vec{x},t)$ shall not be confused with the later mentioned circumferential velocity (u).

POD RESULTS

The Analysis of the POD results can be split into two steps. First, the modal structures and their energy contributions to the flow are investigated. The 2771 discrete velocity fields per measurement result in the same amount of POD modes. Subsequently, the weighting coefficients a_j^i are calculated and their time dependent behavior is investigated.

Figures 11, 12, 13 show the first five Modes. Modal patterns are shown as vectors for the in-plane and as contour plot for the out-of-plane component. As modal patterns are to be compared qualitatively, no quantitative values are given. In addition, as a Mode is generated from all measured flow fields at once, the position of the impeller (and therefore the blades), cannot be drawn. However, both quantification and blade location can be determined from the reconstructed coefficients.

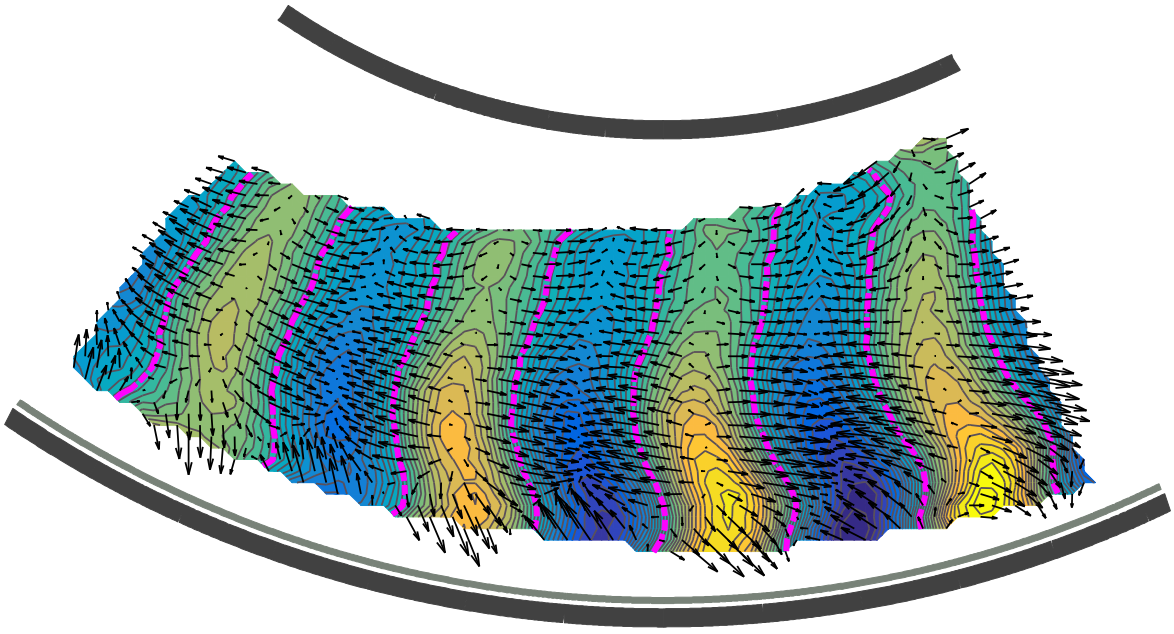

Figure 11: Mode 1

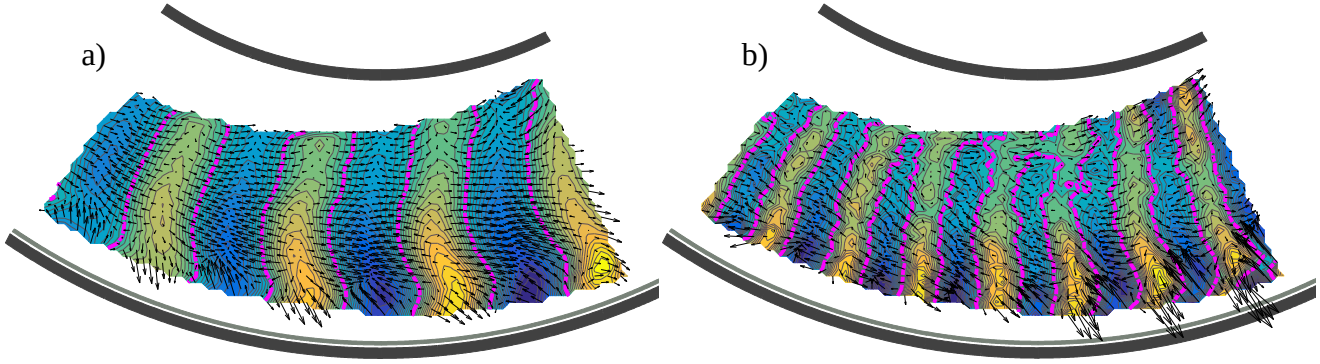

Figure 12 a-b: Mode 2 and 3

The first two modes, as well as Mode 3 and 4, reveal very similar flow patterns. Both pairs show blade related flow structures in plane, as well as out-of-plane, with flow patterns analogous to Figure 9. Modes 3&4 represent the first harmonics of Modes 1&2. They reveal twice as many, but accordingly thinner patterns.

Especially the similarity between Mode 1 and Figure 9 is remarkable. One has to keep in mind that all POD Modes were purely generated out of the raw PIV Images. No additional information, such as angular position of the impeller, or rotational speed was necessary. This is unlike the phase averaging as in Figure 9, were both information were mandatory.

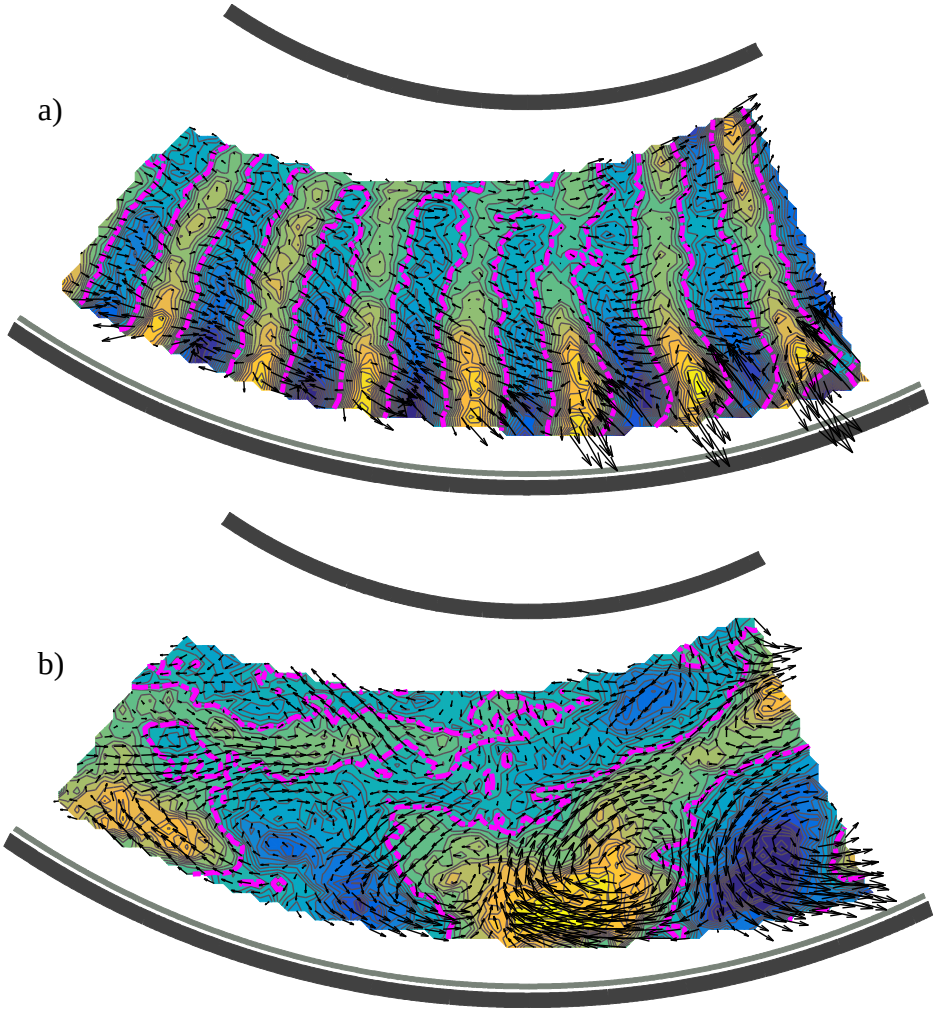

Figure 13 a-b: Mode 4 and 5

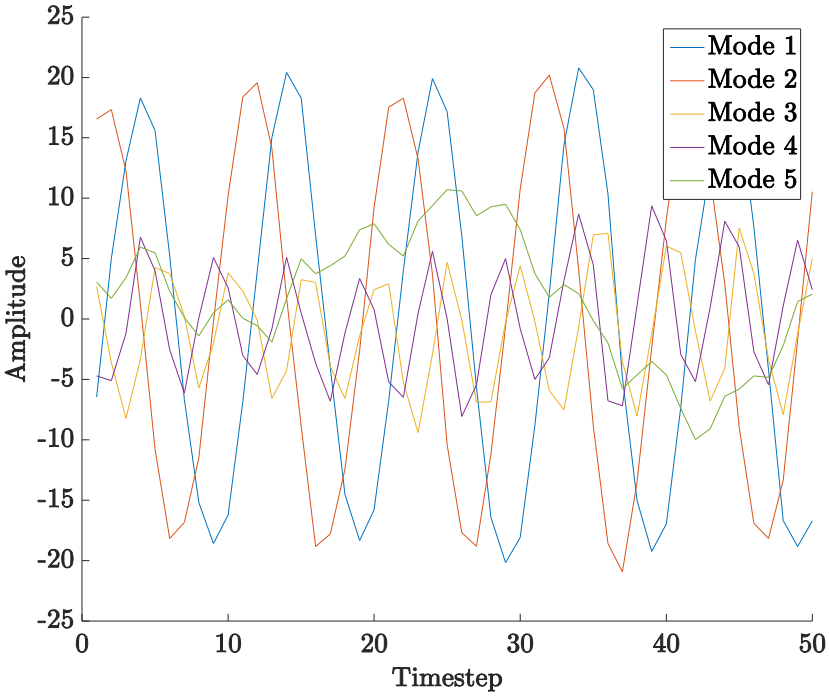

Figure 14: Coefficients of Modes 1 to 4

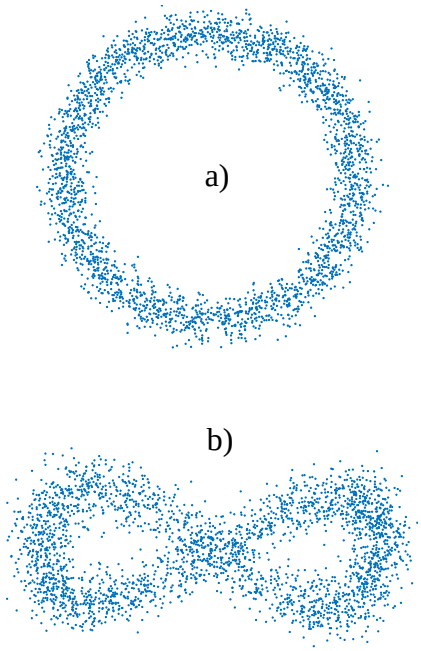

Figure 15: Lissajous figure
a) Mode 1&2 b) Mode 2&3

A distinct difference between Mode 1 and 2 is the fact, that the structures are shifted by a certain angle in flow direction. This 90°-phase shift becomes more obvious from the reconstructed coefficient of the respective modes, as shown in Figure 14. The coefficient oscillation reveals the blade passing frequency of 200 Hz. Note that the 90°-phase shift at identical frequency is verified by the circular shape of the corresponding Lissajous figure of Modes 1&2 (Figure14a). The harmonic characteristic of Modes 3&4 is shown by the doubled frequency in coefficient oscillation compared to Modes 1&2 (Figure 14) and furthermore by the Lissajous figure of Modes 2&3 showing a Lemniscate shape (Figure 15b).

The energy spectrum for the first 20 Modes is introduced with Figure 16. Combined, Modes 1&2 already contain approximately 20% of the flows fluctuation intensity. The directly following Modes 3 and 4 already show a huge decrease in energy. Nevertheless they show the blade related patterns at a doubled frequency and therefore are not to be neglected.

To further understand the physical meaning of the shown modal structures, the retransformation to the temporal domain has to be further analyzed. It explains the similarity between Modes 1 and 2. By alternating between the two shifted structures with blade passing frequency, the visible blade structures and vortex systems

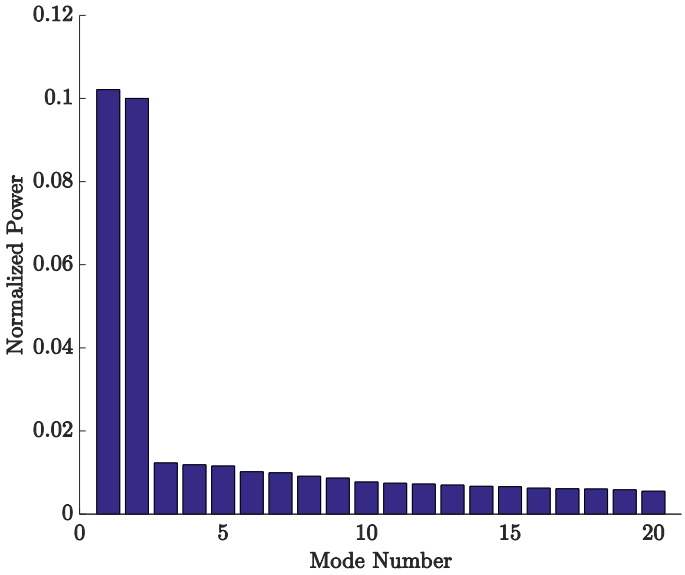

Figure 16: Normalized Mode Power for the first 20 Modes

in either mode are moved through the temporal domain, following the blades. It indicates the driving force behind mass transportation between side channel and impeller.

Mode 5 (see Figure 13b) already contains only about 1% of the total energy. This Mode is added as the strongest of all low-energy bearing Modes, showing no structures obviously related to any parameter of the machine, as well as no oscillation of the coefficient (unlike Modes 1-4) as shown in Figure 14.

From there on, the modal energies asymptotically approach a constant value. This directly indicates a low contribution of correlated information and an increasing influence of noise and turbulence.

CONCLUSION

The understanding of the highly unsteady and complex flow structure within a regenerative pump is crucial for further formulating the energy exchange between the impeller and the fluid. Even high-speed stereo PIV measurements analyzed in a classic approach provide only limited information on the complex three dimensional swirl flows within the machine. The interacting flow patterns, which are the driving force behind the momentum exchange and therefore the working principle of the machine, are concealed by the highly energetic main flow. A simple subtraction of the average flow field from the instantaneous flow field gives a first impression of the vortex structures in game. However, without filtering the results are noisy and can even be misleading in case of sudden random disturbances in the flow field.

By using additional information such as angular positions to do phase averaging, it is possible to switch the point of view from the fixed laboratory system to the rotating blade related system furthermore revealing blade related patterns. However, as mentioned before, phase averaging limits the possibility to discover phenomena to presumed frequencies. With the POD approach this limitation is lifted. Once the predominant average flow field is subtracted, the POD method massively adds to a simpler description of the flow within the machine. Particularly, the entire flow scenario can be approximated in good accuracy with only a few modes of salient flow patterns. Therefore, it is now possible to focus on those structures and, in an upcoming approach, to identify the parameters of the machine generating those specific flow structures. A deeper investigation of those phenomena will be the cause of upcoming projects.

ACKNOWLEDGMENT

This paper is based upon work supported by the German Reasearch Foundation (DFG) under Grant No. 585385; Reference: GA 718/5-1.

BIBLIOGRAPHY

[1] Aubry N “On the hidden beauty of the proper orthogonal decomposition”, Theor. Comput. Fluid Dyn. 2 339–52, **1991**

[2] Adrian, Ronald J. – *Particle-imaging techniques for experimental fluid mechanics*. Annual review of fluid mechanics, 23, 261-304, **1991**

[3] Raffel, Markus, and Christian E. Willert. – *Particle Image Velocimetry a Practical Guide*. 2. Ed. Berlin: Springer, **1998**

[4] Meinhart, Carl D., Wereley, Steve T. & Santiago, Juan G. – *A PIV algorithm for estimating time-averaged velocity fields.* Journal of Fluids Engineering, 122, 285-289, **2000**

[5] Perrin, Rodolphe, Cid, Emmanuel, Cazin, Sebastien, Sevrain, Alain, Braza, Marianna, Moradei, Franck & Harran, Gilles – *Phase-averaged measurements of the turbulence properties in the near*

wake of a circular cylinder at high Reynolds number by 2C-PIV and 3C-PIV. Experiments in fluids, 42, 93-109, **2007**

[6] Van Oudheusden, B.W., Scarano, F., Van Hinsberg, N.P. & Watt, D.W. – *Phase-resolved characterization of vortex shedding in the near wake of a square-section cylinder at incidence.* Experiments in Fluids, 39, 86-98, **2005**

[7] Wernert, P. & Favier, D. – *Considerations about the phase averaging method with application to ELDV and PIV measurements over pitching airfoils.* Experiments in Fluids, 27, 473-483, **1999**

[8] Keller, Jens, Blanco, Eduardo, Barrio, Raúl & Parrondo, Jorge – *PIV measurements of the unsteady flow structures in a volute centrifugal pump at a high flow rate.* Experiments in Fluids, 55, 1-14, **2014**

[9] Ferreira, Carlos, Simão, van Kuik, Gijs, van Bussel, Gerard & Scarano, Fulvio – *Visualization by PIV of dynamic stall on a vertical axis wind turbine.* Experiments in Fluids, 46, 97-108, **2009**

[10] Lourenco, L., Subramanian, S. & Ding, Z. – *Time series velocity field reconstruction from PIV data.* Measurement Science and Technology, 8, 1533, **1997**

[11] Adrian, RJ, Christensen, KT & Liu, Z-C – *Analysis and interpretation of instantaneous turbulent velocity fields.* Experiments in fluids, 29, 275-290, **2000**

[12] A. Cizmas, Paul G. & Palacios, Antonio – *Proper orthogonal decomposition of turbine rotor-stator interaction.* Journal of propulsion and power, 19, 268-281, **2003**

[13] Berkooz, Gal, Holmes, Philip & Lumley, John L. – *The proper orthogonal decomposition in the analysis of turbulent flows.* Annual review of fluid mechanics, 25, 539-575, **1993**

[14] Mattern, P., Gabi, M., Wagner, T., Boehle, M. – *Investigations in a side channel pump using high speed Stereo Particle Image Velocimetry*. 15th Int. Symp. Transp. Phenom. Dyn. Rot. Machinery – ISROMAC-15, Honolulu, **2014**

[15] Mattern, P., Gabi, M., Kriegseis, J. – *Pattern identification in a regenerative pump a combined PIV / POD approach*. The XXII Symposium on Measuring Techniques in Turbomachinery, Lyon, 2014

[16] Kriegseis, J.,Dehler, T., Gnirß, M., Tropea, C., Common-base proper orthogonal decomposition (CPOD) as a means of quantitative data comparison. Meas. Sci. Technol. 21, 085403 (7pp), **2010**

[17] Fernando, J., Kriegseis, J., Rival, D., Modal analysis of confined square and rectangular cavity flows. Int. J. Heat Fluid Flow 47, 123-134, **2014**

[18] Holmes P, Lumley J L and Berkooz G, "Turbulence, Coherent Structures, Dynamical Systems, and Symmetry" (Cambridge: Cambridge University Press), **1996**

[19] Dreyer, Matthieu, Decaix, Jean, Münch-Alligné, Cécile & Farhat, Mohamed – *Mind the gap: a new insight into the tip leakage vortex using stereo-PIV*. Experiments in Fluids, 55, 1-13, **2014**

[20] Graftieaux, Laurent, Michard, Marc & Grosjean, Nathalie – *Combining PIV, POD and vortex identification algorithms for the study of unsteady turbulent swirling flows.* Measurement Science and Technology, 12, 1422, **2001**

[21] Faragallah, W.H., Seitenkanal- Strömungsmaschinen , Verlag und Bildarchiv, Germany,**1992**